CEBAF PROPOSAL COVER SHEET

This Proposal must be mailed to:

CEBAF
Scientific Director's Office
12000 Jefferson Avenue
Newport News, VA 23606

and received on or before OCTOBER 31, 1989

A. TITLE: In-plane Separations and High Momentum Structure in D(e,e'p)

B. CONTACT PERSON: J.M. Finn

ADDRESS, PHONE AND BITNET:

Department of Physics
The College of William and Mary
Williamsburg, VA 23185
Ph #: (804) 253-4471 Bitnet: FINN@CEBAFVAX

C. THIS PROPOSAL IS BASED ON A PREVIOUSLY SUBMITTED LETTER OF INTENT

☒ YES
/ / NO

IF YES, TITLE OF PREVIOUSLY SUBMITTED LETTER OF INTENT

same as above

D. ATTACH A SEPARATE PAGE LISTING ALL COLLABORATION MEMBERS AND THEIR INSTITUTIONS

==========

(CEBAF USE ONLY)

Proposal Received 10-31-89

Log Number Assigned PR-89-026

By KES

contact: Finn

In-plane Separations and High Momentum Structure in D(e,e'p)

THE HALL A COLLABORATION

American University, Cal. State University LA, Case Western Reserve and LANL
Continuous Electron Beam Accelerator Facility
George Washington University, University of Georgia, Indiana University Cyclotron Facility
Kent State University, University of Maryland, Massachusetts Institute of Technology
University of New Hampshire, National Institute of Science and Technology
Norfolk State University, University of Regina, University of Rochester
University of Saskatchewan, Rutgers University, Stanford University
University of Virginia, University of Washington, College of William and Mary
NIKHEF-K, CEN Saclay, University of Clermont-Ferrand
INFN Sezione Sanita, University of Lund

Spokespersons: J.M. Finn (William & Mary), P.E. Ulmer (CEBAF)

Using the capabilities of CEBAF we plan to considerably extend the present knowledge of the basic D(e,e'p) reaction by studying the momentum distribution at higher momentum transfers and by undertaking separations of the R_L, R_T and R_{LT} response functions. The q_μ dependence of the reaction will be examined by performing longitudinal/transverse (L/T) separations for protons emitted along $\vec{q}$ at q_μ^2=0.23, 0.81, 2.14 and 3.41 GeV^2/c^2 at quasifree kinematics ($p_r = 0$). In addition, by detecting protons away from the direction of $\vec{q}$, the angular distribution of emerging protons will be measured for recoil momenta up to 500 MeV/c at a single 3-momentum transfer of 1.0 GeV/c. From in-plane measurements on either side of $\vec{q}$ plus a backward angle measurement the R_T, R_{LT} and $R_L + R_{TT}$ components can be determined. This should provide additional checks on the model dependence of the reaction.

Date	Description	Beam Hours	Energies	Max. Luminosity
Oct. 31, 1989	^{1,2}H(e,e'p)	554	0.4–4.0 GeV	1.4×10^{38}cm^{-2}sec^{-1}

1 Introduction and Motivation

The deuteron provides the most direct measure of the nucleon-nucleon force and its relative simplicity allows for detailed calculations of the reaction. Understanding deuterium is of vital importance for the study of heavier nuclei since it serves as a basis for realistic nucleon-nucleon (NN) interaction models. Although deuterium is among the few targets studied by (e,e'p) measurements, present knowledge is fragmentary. In fact, other than a very low energy experiment performed at Tohoku University[1] a separation of the electromagnetic response functions in (e,e'p) has never been performed for this target. The most extensive study to date is a measurement of the momentum distribution by the Saclay group in the region $0 \leq p_r \leq 300$ MeV/c.[2] Turck-Chieze *et al.* have also studied the contribution of Δ mechanisms at high recoil momentum (up to 500 MeV/c) for $x < 1$.[3] Recent developments include unpublished measurements at NIKHEF involving separations at low $\vec{q}$ (330–360 MeV/c) for recoil momenta up to 200 MeV/c[4] and an approved experiment at Bates proposing to undertake separations and measurements of out-of-plane observables at a few selected kinematics[5]. The most precise measurement on the analogous (p,2p) reaction differs from the (e,e'p) reaction by more completely satisfying the sum-rule but shows substantial differences in the response at high recoil momenta, presumably due to differences in the reaction mechanism.[6] Our proposal differs from previous (e,e'p) measurements by exploiting the dynamical range available at CEBAF to explore the reaction over a large range of $\vec{q}$ and to high recoil momentum. This initial study proposes to examine the in-plane response functions in the region of the quasielastic peak ($x = 1$). Both the $\vec{q}$ dependence (at $p_r = 0$) and the recoil momentum dependence (at $\vec{q} = 1$ GeV/c) will be explored. It is envisioned that the complete program will include non-quasifree kinematics ($x \neq 1$), out-of-plane measurements and measurements of spin observables. A separate proposal to study polarization transfer in D($\vec{e}$,e'$\vec{p}$) is being submitted by the Hall A collaboration.

In the One Photon Exchange Approximation (OPEA) the unpolarised (e,e'p) cross section can be written in terms of four independent nuclear structure functions[7]:

$$\frac{d^4\sigma}{d\omega d\Omega_e dT_p d\Omega_p} = \sigma_M \left[v_L R_L + v_T R_T + v_{LT} R_{LT} \cos\phi_z + v_{TT} R_{TT} \cos 2\phi_z \right]. \quad (1)$$

The more general case, including beam and recoil polarization has been worked out in detail.[8] The response functions depend on $\vec{q}$, ω, T_p (the proton kinetic energy) and θ_x (the proton angle with respect to $\vec{q}$). ϕ_x is the angle between the electron scattering plane and the plane containing $\vec{q}$ and the detected proton. The v's are known kinematic factors weighting the various virtual photon polarization states and σ_M is the cross section for scattering from a structureless Dirac particle. The response functions, R, represent various products of components of the nuclear electromagnetic current. By varying the kinematics so as to keep the response functions fixed, each may be separately determined isolating various components of the nuclear electromagnetic current. In-plane measurements are capable of separating the R_T and R_{LT} term from a linear combination of the R_L and R_{TT} terms. At quasifree kinematics the R_{TT} term tends to be small.

Fabian and Arenhövel[9] have performed a nonrelativistic theoretical treatment of the (e,e'p) reaction for the case of the deuteron, including effects from Final State Interactions (FSI), Meson Exchange Currents (MEC) and Isobar Configurations (IC). A calculation of the four unpolarized response functions for $\vec{q} \sim 1$ GeV/c and quasielastic kinematics ($x = 1$) is shown in Figure 1.[10] These kinematics are very close to those of our angular distribution study described below. The R_{TT} term which can only be separated via an out-of-plane measurement is quite small and therefore may be neglected in the context of this model. In Figure 2 the asymmetry relative to $\vec{q}$ as deduced from the four response functions in Figure 1 is shown vs θ_{pn}^{cm}. Measurements above $\theta_{pn}^{cm} \sim 30°$ will provide a sensitive test of FSI models. Although the calculations are nonrelativistic, they serve as a guide for the experimental program at CEBAF. Additional calculations of the effects of MEC and FSI on the angular distribution and polarization of protons in D(e,e'p) have been undertaken by groups in the USSR and France.[11] Furthermore, fully relativistic calculations are currently underway by Van Orden and Gross.[12] In all, four theoretical groups have expressed interest in performing calculations for deuterium at CEBAF kinematics.

For the special case $\theta_x = 0$ (parallel kinematics) only the longitudinal, R_L, and transverse, R_T, response functions survive. One of the many open questions which (e,e'p) measurements hope to answer is the nature of the electromagnetic form

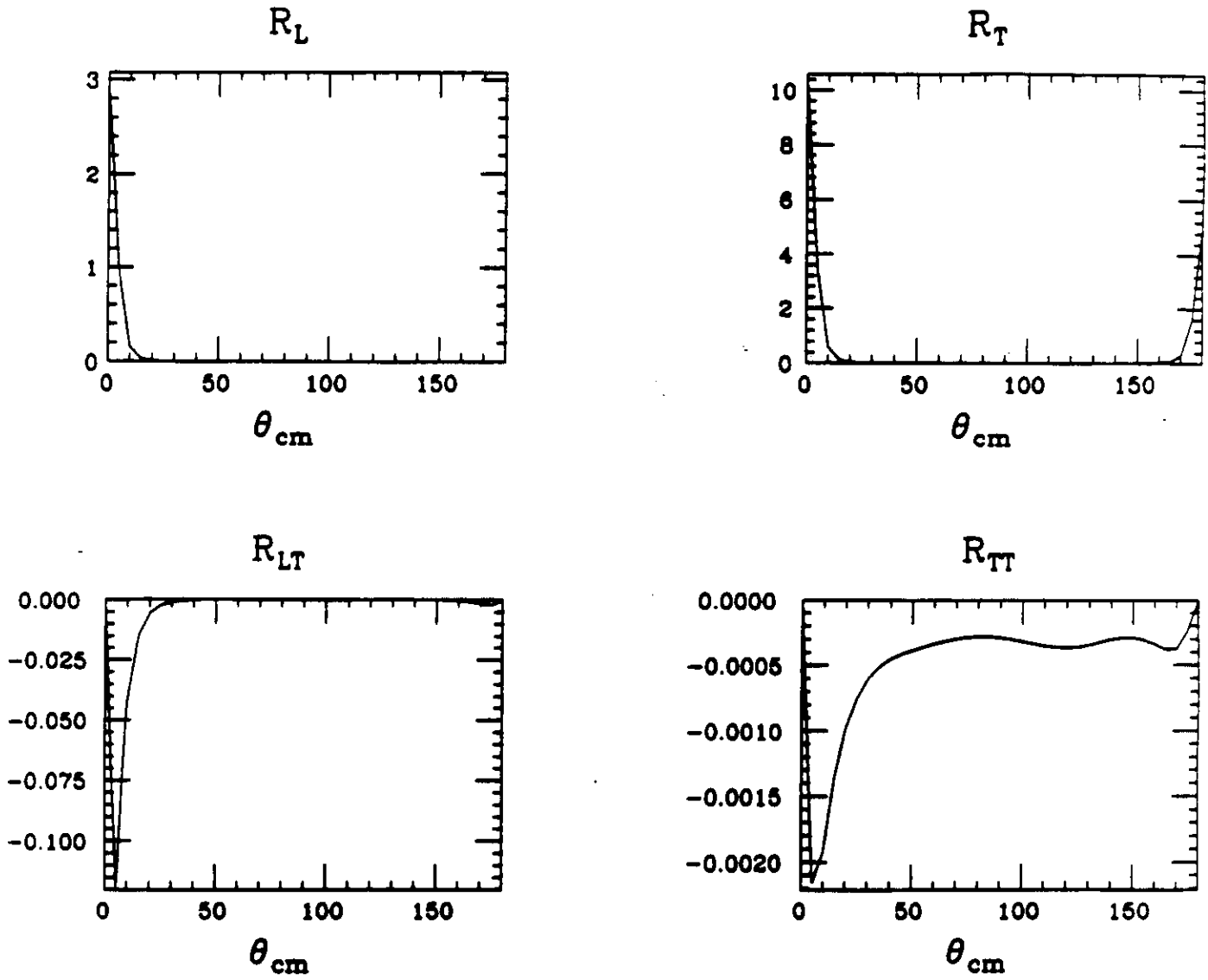

Figure 1 The four unpolarized response functions as calculated by Arenhövel for $\vec{q} \sim 1$ GeV/c and quasielastic kinematics ($x = 1$).

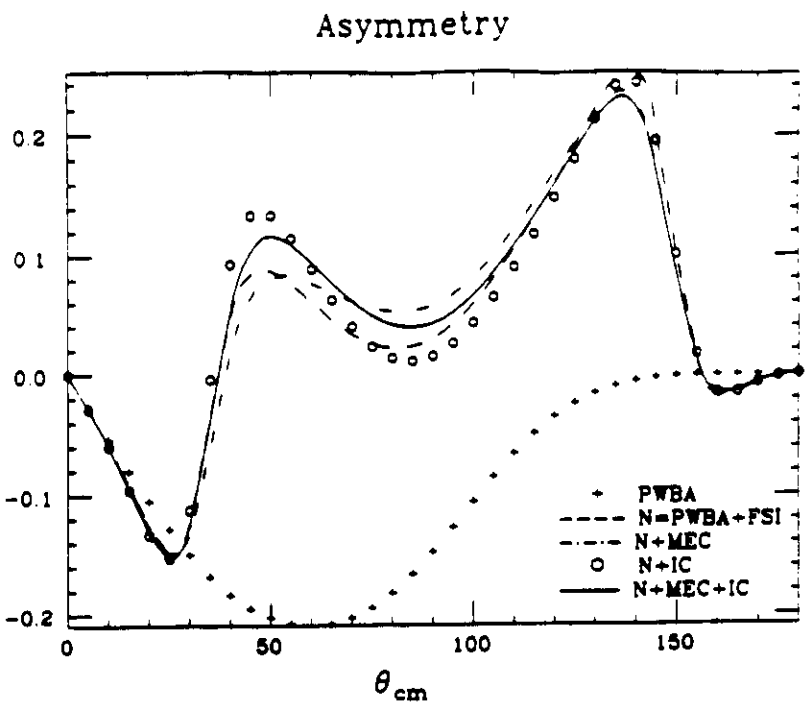

Figure 2 The asymmetry $(= [\sigma(\phi_z = 0) - \sigma(\phi_z = \pi)]/[\sigma(\phi_z = 0) + \sigma(\phi_z = \pi)])$ relative to $\vec{q}$ as deduced from the four response functions of Figure 1.

factors of nucleons embedded in the nuclear medium. A longitudinal/transverse separation can provide a characterization of these form factors in a more complete way than, for example, differential cross section measurements alone. Although no such measurements have been published for deuterium, separations have been carried out for other nuclei at Bates[13], NIKHEF[14] and Saclay[15]. The presence of additional reaction components in the quasielastic region can cloud the simple interpretation of the coincidence response functions in terms of purely nucleonic properties. The Bates measurement[13] suggests the presence of such currents above the two-particle emission threshold. A more systematic study over an extended kinematical domain will be needed to quantify the relative importance of two-body or many-body effects and nucleon modifications and CEBAF will be an invaluable tool in this effort. CEBAF will afford the opportunity to study the behavior of these response functions to momentum transfers higher than those possible at existing laboratories and with much greater statistical precision. High resolution spectrometers are clearly crucial for these measurements since systematic errors in the cross section are magnified in determining R_L and R_T. The longitudinal response function becomes especially difficult to determine accurately above momentum transfers of 2 GeV/c due to its small relative size.

An orthogonal set of measurements consists of examining the angular distribution of emerging protons out to large internal momenta. The high momentum components of the wave function are expected to be sensitive to effects of correlations arising from the short range part of the nucleon-nucleon interaction.[16] An important correction to the cross section is the FSI which may have spin-orbit contributions. These effects can be studied by separating the individual response functions. For example one can measure the σ_{LT} asymmetry relative to the $\vec{q}$ direction by making measurements at $\phi_z = 0$ and π. This asymmetry is sensitive to the off-mass-shell parameterization of the elementary *ep* cross section as well. By making an additional measurement at a backward electron angle one can determine the R_T term as well.

Using the capabilities of CEBAF we plan to considerably extend the present knowledge of the basic D(e,e'p) reaction by studying the momentum distribution at higher momentum transfers and by undertaking separations of the R_L, R_T and R_{LT} response functions. In what follows two sets of measurements in D(e,e'p) are described: a longitudinal/transverse separation in quasifree kinematics for protons emitted along $\vec{q}$ at q_μ^2 of 0.23, 0.81, 2.14 and 3.41 GeV^2/c^2 and a measurement of the angular distribution of protons up to 500 MeV/c recoil. The lowest q_μ separation point is included to match on to measurements expected to be undertaken at existing facilities. The angular distribution measurements are made at the top of the quasielastic peak ($x = 1$) holding the momentum transfer and the invariant mass constant thereby fixing the relative momentum in the center of mass of the recoiling proton-neutron pair. For a given recoil momentum the virtual photon longitudinal polarization is varied by making forward and backward angle measurements and the LT interference response function is separated by detecting protons on either side of $\vec{q}$ at the forward electron angle. To minimize energy changes we have selected our kinematics to use energies which are multiples of the maximum single-pass energy of 800 MeV. Ignoring the energy of the injector this gives a five-pass energy of 4 GeV. By doing this all the measurements can be made at a single machine energy of 4 GeV, except for the backward angle energy of 400 MeV at the lowest q_μ^2 point which can be reached with a five pass energy of 2 GeV.

2 Models for Counting Rate and Background Estimates

The (e,e′) cross sections were calculated with the computer code, QFSV[17] which employs a Fermi gas model to compute the quasielastic component and includes contributions from the Delta and higher resonances. The (e,p), (e,π^+) and (e,π^-) cross sections were calculated with the electro-production code, EPC.[17] The (e,p) cross section is approximated by the (γ,p) cross section times a factor corresponding to the virtual photon flux:[18]

$$\frac{d^2\sigma}{d\Omega_p dE_p} = \frac{N_v(\omega)}{\omega_0} R \frac{d\sigma_\gamma}{d\Omega_p} \tag{2}$$

This assumes the dominance of the transverse component and the forward peaking approximation (FPA) since most virtual photons arise from near 0° scattering of the electron. Here, R is a recoil factor and ω_0 is the energy transfer in the FPA. $N_v(\omega)$ is the virtual photon spectrum.[18] For deuterium the (γ,p) cross section for scattering to the pn channel is taken from a fit to deuteron photodisintegration data.[19] For the quasifree pion production region a Breit-Wigner form was used in the Delta region with appropriate angular dependences, and above that the cross section was assumed to be uniform and isotropic in the center-of-mass frame.

The (e,e′p) cross sections were calculated with the computer code MCEEP.[20] This code performs a folding of the cross section over the experimental acceptances and gives realistic count rate estimates for any desired kinematical cut. The nuclear model used for the present count rate estimates assumes the validity of the Plane Wave Impulse Approximation (PWIA); thus, the (e,e′p) cross section factors into an elementary ep off-shell cross section times a quantity which contains the nuclear structure information, the spectral function[21]:

$$\sigma_{exp} = K\sigma_{ep}\frac{1}{\eta}S(\vec{p}_r, E_m) \tag{3}$$

where K is a kinematical factor. The recoil factor, η, for scattering to a bound state of the residual nucleus is given by

$$\eta = 1 - \frac{E'}{E_r}\frac{\vec{p}' \cdot \vec{p}_r}{|\vec{p}'|^2} \tag{4}$$

where E' (E_r) is the total energy of the detected proton (recoiling system) and $\vec{p}'$ is the proton final momentum. The spectral function, S, represents the joint

probability for finding within the nucleus a proton of momentum $-\vec{p}_r$ and separation energy E_m. In PWIA, all of the dependence on virtual photon polarization is contained within the ep cross section. Many ambiguities exist in the extrapolation of the on-shell cross section to that for a bound proton. However, all prescriptions are fairly consistent for protons which are nearly on-shell. Here, the "CC1" prescription of de Forest is used for σ_{ep}[22]. The bound state spectral function is given by

$$S(\vec{p}_r, E_m) = |\phi(p_r)|^2 \delta(E_m - E_a) \tag{5}$$

where E_a (=2.2 MeV) is the binding energy of deuterium. The $|\phi(p_r)|^2$ are taken from the parameterization of Krautschneider[23]:

$$|\phi_D(p_r)|^2 = 4\pi N \left(\frac{1}{T_1} - \frac{1}{T_2}\right)^2 \tag{6}$$

with

$$\begin{aligned} T_1 &= p_r^2 + k_1 \\ T_2 &= p_r^2 + k_2. \end{aligned} \tag{7}$$

The constants $k_1 = 2088$ (MeV/c)^2 and $k_2 = 67600$ (MeV/c)^2 reproduce the shape of the experimental distribution up to $p_r \sim 300$ MeV/c quite well. The distribution was normalized to yield one proton (N=0.638 MeV/c). Figure 3 compares this shape with the data of Bernheim *et al.*[2] Also shown in the figure is the deuteron momentum distribution derived from the NN interaction of the Paris potential.[24] Below p_r=300 MeV/c the Paris and Krautschneider parameterizations are nearly identical.

Although these models are admittedly crude, they serve to evaluate the feasibility of performing experiments at CEBAF. Certainly, more realistic calculations will be required in order to draw conclusions from data and such calculations are currently underway by Van Orden and Gross.[12]

3 Analysis of Errors

Uncertainty in the determination of the particle coordinates at the spectrometer focal planes is expected to be the dominant source of systematic error since the (e,e'p) cross section varies rapidly within the acceptances of the spectrometers. The computer code SIGEEP[25] was used to estimate the sensitivity of the (e,e'p)

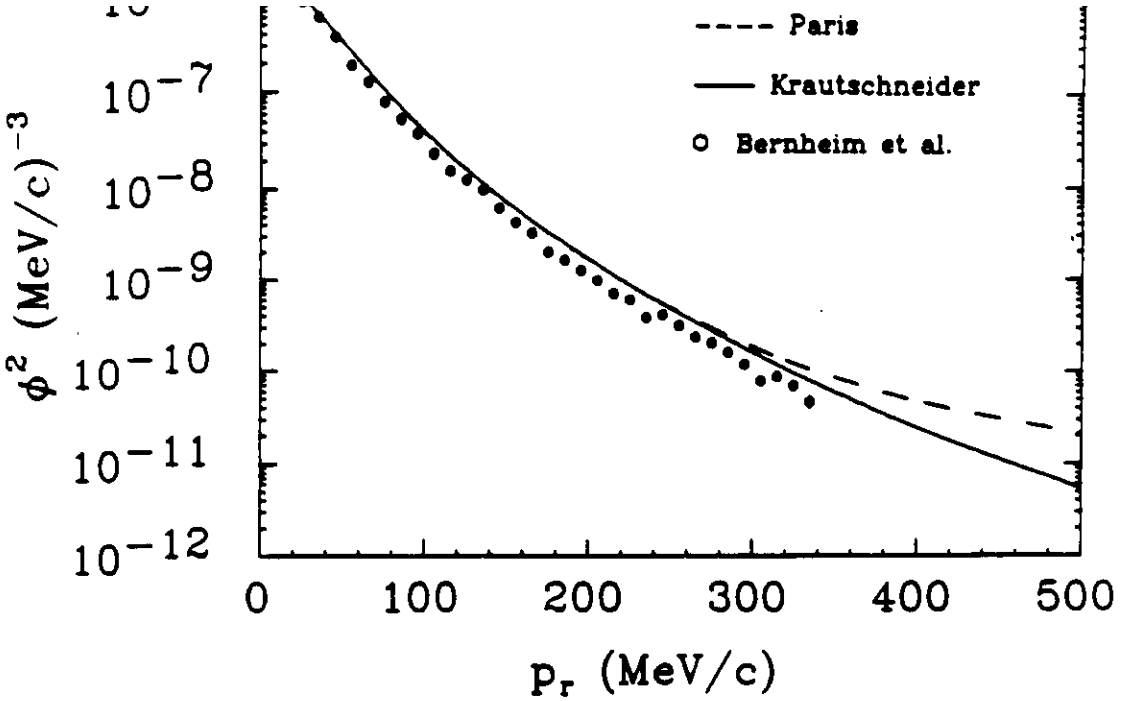

Figure 3 Deuteron momentum distribution as measured by Bernheim *et al.*[2]. Also shown are the Krautschneider and Paris parameterizations.

cross section to kinematical variables determined from the focal plane coordinates. This was accomplished by numerically computing the derivatives of the factorized PWIA expression for the cross section with respect to the detection angles and momenta of the particles. While statistical errors tend to average to zero, systematic errors must be controlled across the focal planes to a very high degree of accuracy. For example, knowledge of the central spectrometer angle is not sufficient because of the rapid variation of the cross section over the angular acceptance.

Other sources of error which have been ignored in this analysis include uncertainties in target thickness and beam current. Since the emittance of the beam is expected to be very low and since beam dispersing systems are not likely to be part of the initial complement of equipment, effects of local beam heating on gas targets and consequent density variations may be important. Luminosity monitors accurate to the fraction of a percent level will therefore be required. Samples of the single-arm cross sections will be used as an internal check on luminosity variations.

4 Targets

High power target cells similar to those needed for these measurements are being developed by members of the Hall A collaboration. A minimum of two cells are required, one liquid hydrogen and one liquid deuterium. These targets should be capable of handling 200 μA maximum beam current on a 10 cm long cell. Because of the need for precision we plan on restricting the maximum beam current to 50 μA (for a maximum luminosity of 1.4×10^{38} cm^{-2}sec^{-1}) for this experiment. In addition, we will need to have CH_2 and ^{12}C targets in the ladder for additional normalization checks. Also, a BeO screen will be required for alignment checks. A helium refrigerator of up to 150 Watts cooling power will also be needed (50 μA on 1.5 g/cm^2 of deuterium). Counting rates assume a luminosity of 1.4×10^{38} cm^{-2}sec^{-1}.

5 Longitudinal/Transverse Separations

The L/T separation measurements are of fundamental importance in disentangling the various contributions to the reaction and require no special apparatus in addition to the two spectrometers (*e.g.* polarimeters or out-of-plane capability). Each measurement employs parallel kinematics (outgoing proton detected along $\vec{q}$, the three momentum-transfer) so that the interference response functions do not contribute. Averaging over a symmetric ϕ_z range, the cross section reduces to a sum of two terms:

$$\frac{d^4\sigma}{d\omega d\Omega_e dT_p d\Omega_p} = K'\sigma_M \left[\frac{2q_\mu^2}{\vec{q}^2}\epsilon R_L + R_T\right]. \tag{8}$$

where K' is a kinematical factor and ϵ is the longitudinal virtual photon polarization defined as

$$\epsilon = \left[1 + \frac{2\vec{q}^2}{q_\mu^2}\tan^2(\theta/2)\right]^{-1}. \tag{9}$$

To carry out these measurements it is important that the spectrometers be able to reach small forward angles $\sim 12.5°$. Small electron angles allow us to maximize the longitudinal polarization and cross sections while for backward electron angles

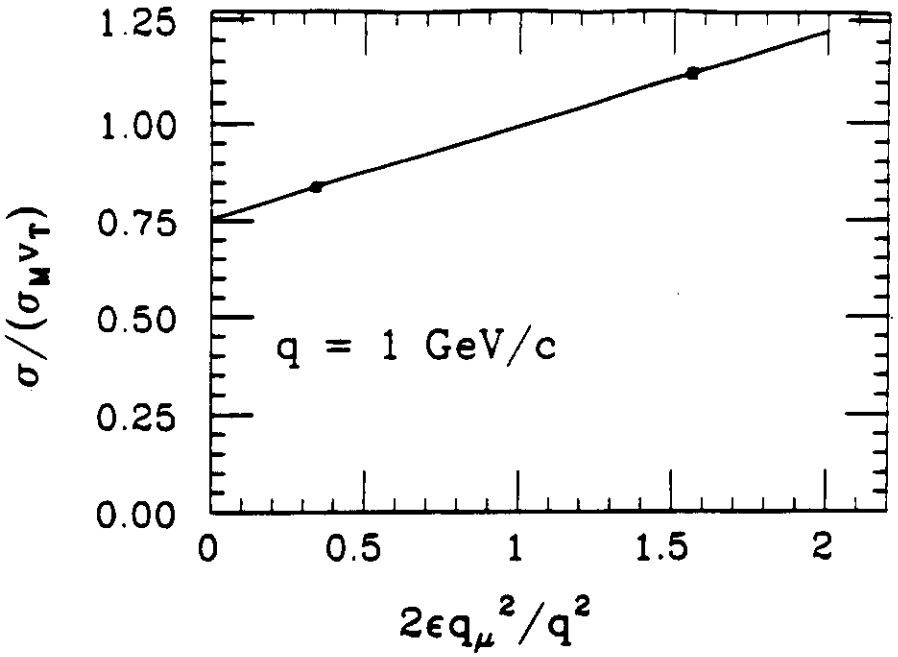

Figure 4 Illustration of extraction of R_L and R_T by a Rosenbluth separation at a 3-momentum transfer of 1 GeV/c. The error bars on the data points are for nominal 1% errors. The intercept of the curve yields R_T to an accuracy of 1.3% while the slope yields R_L to 4.5% accuracy.

Table 1

Kinematics for L/T Separations

Kin	q_μ^2 GeV^2/c^2	e MeV	ω MeV	T_p MeV	θ deg	θ_p deg	ϵ
IF	0.234	1600.	127.1	124.9	18.12	−66.40	0.9484
IB		400.			94.08	−32.98	0.289
IIF	0.811	4000.	435.2	433.0	13.69	−57.55	0.966
IIB		800.			112.88	−19.64	0.151
IIIF	2.139	4000.	1144.9	1142.7	25.00	−40.51	0.863
IIIB		1600.			117.96	−12.50	0.101
IVF	3.408	4000.	1822.9	1820.7	36.46	−29.91	0.700
IVB		2400.			103.33	−12.50	0.137

the proton tends to be emitted at small forward angles. Figure 4 illustrates the method of performing a Rosenbluth separation for a typical kinematics.

We examined four values of momentum transfer. The kinematics are given in Table 1 and are centered at recoil momentum, $p_r = 0$. In arriving at these kinematics, minimum momenta of 0.27 GeV/c and minimum angles of 12.5° were assumed for

both spectrometers. The $q_\mu^2 = 0.234$ GeV^2/c^2 ($\vec{q} = 0.5$ GeV/c) point is included to match on to measurements which can be performed at existing facilities. In addition, a maximum beam energy of 4 GeV was assumed. A larger beam energy would be advantageous for the higher $\vec{q}$ points since it would allow more forward electron angles giving higher counting rates and better virtual photon polarization lever arms.

Counting rates were based on the spectrometer acceptances given in Table 2 where $\theta_{V(H)}$ is the vertical (horizontal) spectrometer angular acceptance. The calculated cross sections were integrated over the momentum acceptance of the spectrometers to arrive at the counting rates. The results of the single-arm cross section calculations for kinematics IIF are shown in Figure 5a, 5b and 5c. For each kinematics, the integrated cross sections and rates are given in Tables 3 and 4 respectively. All rates assume a luminosity of 75 μA-g/cm^2 ($= 1.4 \times 10^{38}$ cm^{-2}sec^{-1}) and a coincidence resolving time of 2 ns (full width at base) is assumed for the accidentals rates. The timing resolution is expected to be better than 2 ns but this will not improve the signal-to-noise ratio because of the 2 ns substructure of the beam. The accidentals rates and signal-to-noise exclude contributions from $\pi^\pm$ and therefore assume good particle identification in both arms. To achieve the required high rejection ratios for pions we plan to use both shower and Čerenkov counters in the focal plane. From Table 4, the instantaneous counting rates are not expected to be a problem from the point of view of π rejection. A rejection ratio of $\sim 10^5$ is necessary for the worst case. The accidentals rates are calculated assuming cuts in missing mass (a resolution of 1 MeV is assumed), ω and making use of the excellent vertex resolution ($\pm$ 1 mm) of the spectrometer pair. While the resulting signal-to-noise ratios are excellent for the L/T measurements, and therefore not tabulated, all these cuts are necessary for the angular distribution measurements at high recoil momentum. The singles rates are very reasonable except at the lowest q_μ^2 point where we plan to run at reduced luminosity. The coincidence yield is shown after cuts; the uncut yield is significantly larger at the forward angles. This may create some data processing bottlenecks at the lowest q_μ^2 points but the times involved in these measurements are minimal.

In general, correlated backgrounds from (e,e'π^+) and (γ,π^-p) need to be considered as well. (Uncorrelated events can be eliminated by background subtraction

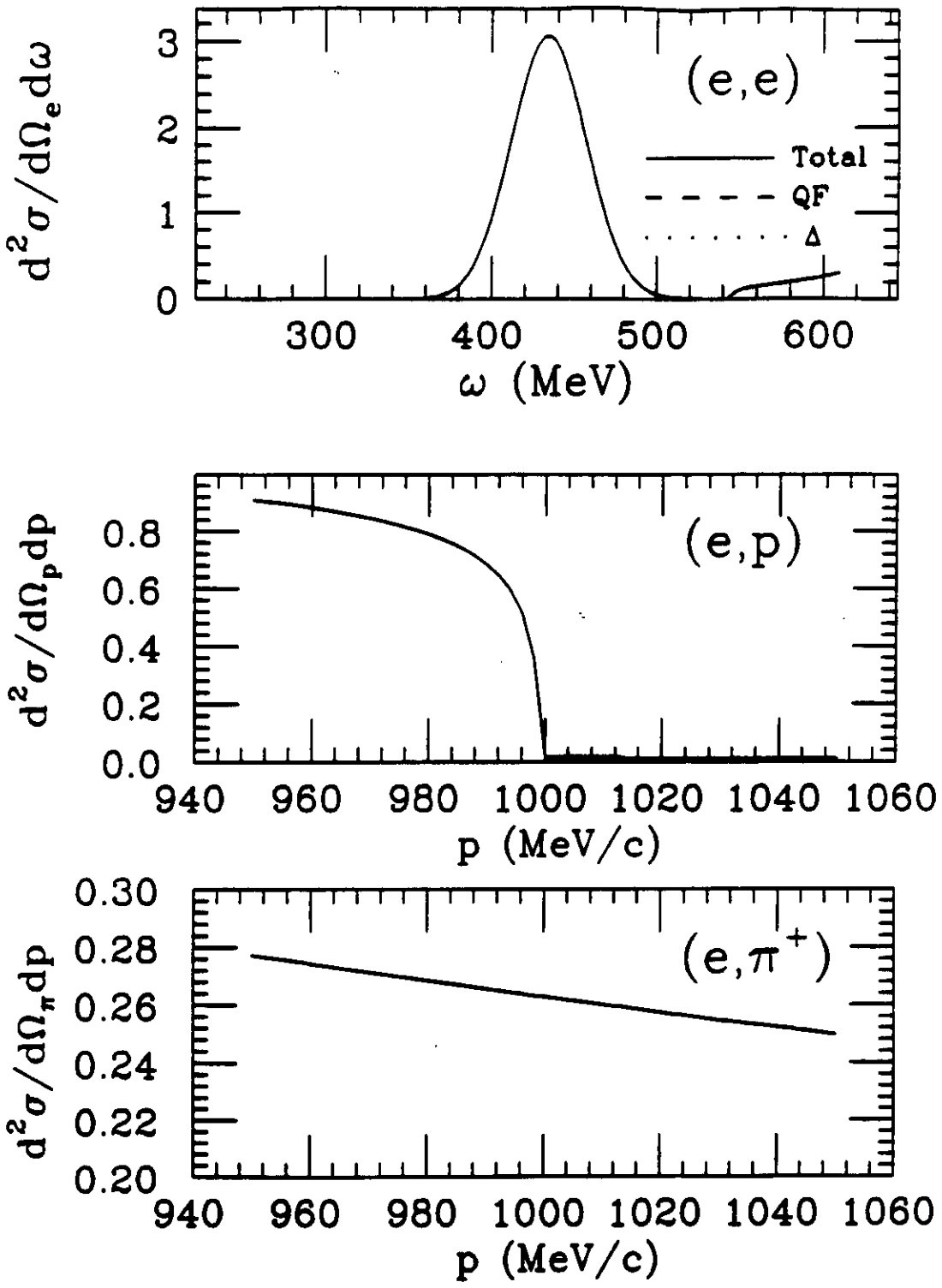

Figure 5 Single-arm cross sections for kinematics IIF. a) The (e,e′) cross section; b) The (e,p) cross section; c) The (e,π^+) cross section in the proton arm. The (e,π^-) cross section (not shown) is small compared to the (e,e′) cross section at this kinematics. Cross sections are in units of nb/MeV/c/sr.

Table 2

Assumed Spectrometer Acceptances

Quantity	Electron Arm	Proton Arm
momentum	±5%	±5%
θ_V	±65 mr	±65 mr
θ_H	±30 mr	±30 mr

Table 3

Integrated Cross Sections for L/T Separations

Kinematics	(e,e′) nb/sr	(e,π^-) nb/sr	(e,p) nb/sr	(e,π^+) nb/sr	(e,e′) w/cuts
IF	1480	6.70	56.8	16.2	1160
IB	28.0	0	22.6	0	28.0
IIF	186	15.5	39.6	26.8	99.4
IIB	0.818	0.250	24.2	0	0.818
IIIF	2.03	14.3	462	29.1	0.720
IIIB	0.0155	1.33	396	0	0.0155
IVF	0.118	13.2	325	8.28	0.0368
IVB	0.00278	2.89	294	0	0.00278

Table 4

Counting Rates for L/T Separations

Kin.	(e,e′) sec^{-1}	(e,e′) w/ ω cut sec^{-1}	(e,π^-) sec^{-1}	(e,p) sec^{-1}	(e,π^+) sec^{-1}	trues sec^{-1}	accidentals sec^{-1}
IF	1630000	1280000	7370	62500	17900	16000	6.38×10^{-1}
IB	30900	30900	0	24800	0	3080	6.13×10^{-3}
IIF	205000	109000	17000	43600	29500	883	2.65×10^{-2}
IIB	900	900	275	26600	0	349	1.33×10^{-4}
IIIF	2230	791	15700	508000	32000	30.2	1.75×10^{-3}
IIIB	17.1	17.1	1460	436000	0	17.1	3.24×10^{-5}
IVF	130	40.5	14500	358000	9110	6.06	5.01×10^{-5}
IVB	3.06	3.06	3180	324000	0	3.34	3.42×10^{-6}

but event-by-event recognition will be desirable to enhance the signal-to-noise

ratio.) For the case at hand where the kinematics are quasielastic, $(\gamma, \pi^- p)$ requires a photon energy near the endpoint. Thus, we do not expect this process to dominate the correlated yield. Furthermore, the $(e,e'\pi^+)$ process is not allowed kinematically for these experiments. Hence, for now these correlated backgrounds are neglected although it would be desirable to have actual estimates in the future.

In Figure 6 the time-of-flight of various particles relative to that for electrons is shown for a 25 meter spectrometer flight path. Assuming one has particle identification in the electron arm, particle ID can be achieved in the proton arm via a time-of-flight measurement relative to the electron. This holds only for the correlated coincidence backgrounds. To allow independent operation of the spectrometers and for redundancy (as well as to maximize the signal-to-noise ratio), standalone particle identification in both arms is needed. For the cases studied a π rejection ratio of 10^5 is required.

In performing the separation, cuts must be applied for each measurement to insure that comparable ranges of each physical variable are sampled for both electron angles. The first order cut will consist of restricting the range of energy transfer, ω, for the forward angle run to match that for the backward angle. In addition, only comparable regions of recoil momentum should be compared in performing the separation. This is accomplished by matching the angular phase space about the central $\vec{q}$ direction for the two kinematics. The ranges considered and the corresponding coincidence counting rates are given in Table 5. The range of p_r is shown but no explicit cut was made on this variable. $\Delta\theta_q^{H(V)}$ represents the cuts made on the horizontal (vertical) variation about the central $\vec{q}$ direction. The yield distributions versus recoil momentum as calculated by MCEEP are shown in Figure 7 for Kinematics IV before and after cuts. The yields for the backward (forward) electron angle are shown as a solid curve (histogram). The cuts result in a good matching of the distributions at both kinematics as is required for separation measurements. Running times were calculated assuming 1% statistics (average per 10 MeV/c bin in p_r). Since the cross sections do not include radiative effects, we have estimated radiative correction factors of 30% and 20% for the forward and backward angle measurements respectively and have increased our total time estimate accordingly. It is seen that adequate statistics can be acquired in a reasonable amount of time even at the highest momentum transfer.

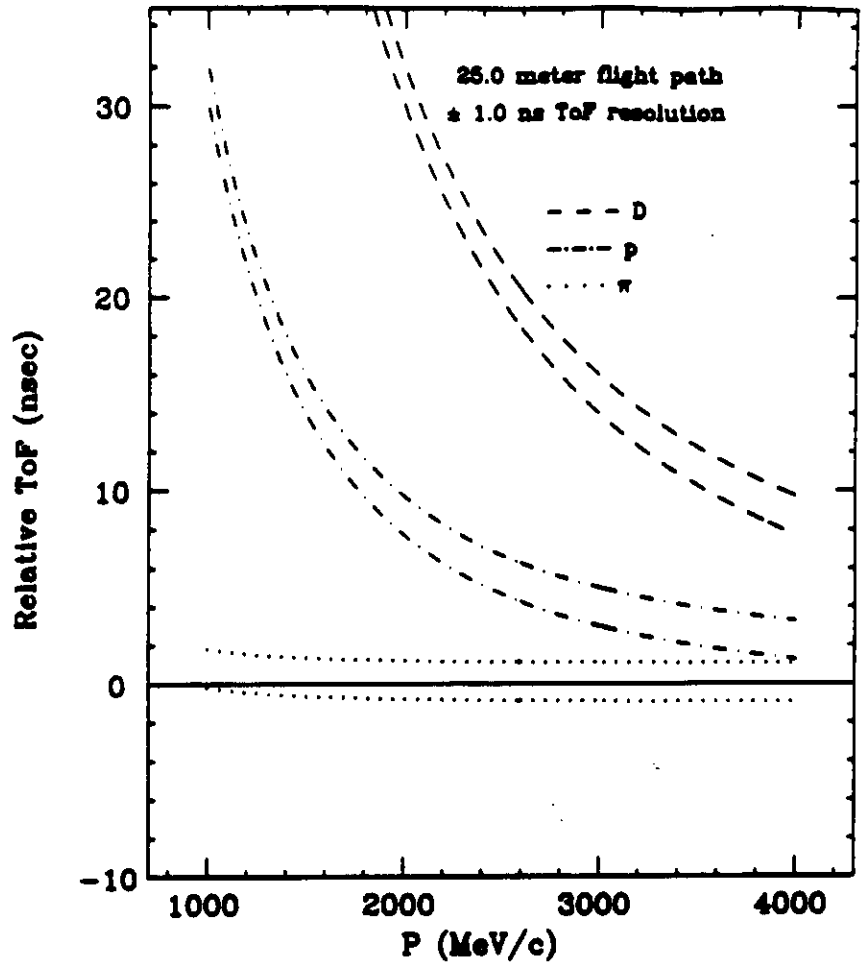

Figure 6 Time-of-flight relative to electron arrival time for a 25 meter flight path. The error band is for a nominal ± 1 ns timing resolution.

Using SIGEEP a sensitivity analysis was performed to estimate the uncertainty in the (e,e'p) cross section due to uncertainties in the momenta and angles of the detected particles. The total error is computed assuming the measurement uncertainties given in Table 6; the results are given in Table 7. The error estimates are computed assuming these quantities are known to this precision in an absolute sense. The method of determining absolute energies of both the beam and detected particles to these levels must be clearly established for these estimates to apply. At quasielastic kinematics (p_r = 0) kinematical sensitivities with respect to a global shift are minimized since the momentum distribution is averaged over symmetrically. However, for a particular p_r range the uncertainty will be significantly larger. In addition, correlated errors in the spectrometer field map across the acceptance will partially destroy this symmetric averaging and result in larger

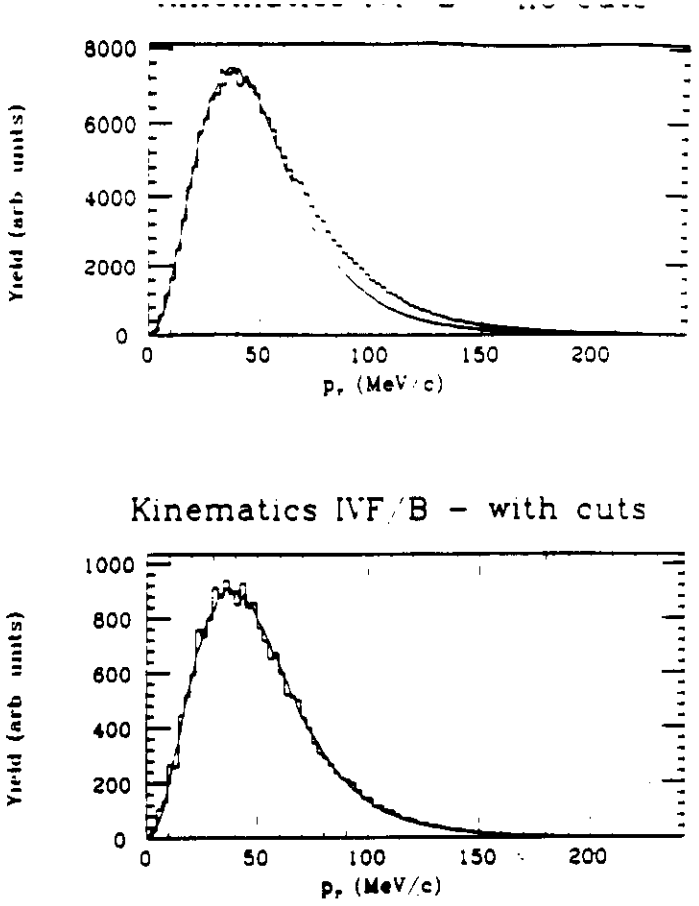

Figure 7 Yield distributions versus p_r as calculated by MCEEP for Kinematics IV before and after cuts. The yields for the backward (forward) electron angle are shown as a solid curve (histogram).

Table 5

Coincidence Rates and Counting Times with Cuts

Kinematics	ω range MeV	$\Delta\theta_q^V$ ± mr	$\Delta\theta^H$ ± mr	p_r range MeV/c	trues (sec^{-1})	Time (hours) $L_{max} = 75\mu$A-g/cm^2
IF	113–141	36	20	0–40	16000	< 0.1
IB					3080	< 0.1
IIF	417–453	22	20	0–60	883	< 0.1
IIB					349	< 0.1
IIIF	1122–1168	16	10	0–80	30.2	0.8
IIIB					17.1	1.3
IVF	1794–1852	18	10	0–100	6.06	4.6
IVB					3.34	8.1
TOTAL						15.2
TOTAL incl. rad. corr.						19

errors. For the L/T separations, the electron final energy must be determined to an accuracy of $\sim 1\times 10^{-3}$ to restrict the error in the cross section from this variable alone to 1%. The incident (scattered) electron angle must be determined to 2 mr (3 mr) for the same error. For the proton angle the requirement is not as stringent; 8.0 mr is sufficient for the above cases. However, these requirements become more stringent as one moves away from $p_r = 0$ as will be seen in the second phase where the recoil momentum dependence is examined.

Table 6

Assumed Measurement Uncertainties

Variable	Uncertainty
e	$\pm 1 \times 10^{-4}$
e'	$\pm 1 \times 10^{-4}$
θ_b	± 0.1 mr
θ	± 0.1 mr
θ_p	± 0.1 mr

Table 7

Systematic Uncertainties in Cross Section

Kin.	e %/MeV	θ_b %/mr	e' %/MeV	θ %/mr	θ_p %/mr	Total Error %
IF	1.7	0.069	0.37	0.39	0.097	0.28
IB	1.6	0.0047	0.27	0.025	0.082	0.063
IIF	0.53	0.64	0.17	0.19	0.13	0.23
IIB	0.54	0.060	0.064	0.0070	0.059	0.044
IIIF	0.28	0.54	0.068	0.20	0.069	0.13
IIIB	0.29	0.013	0.013	0.0031	0.018	0.047
IVF	0.22	0.42	0.013	0.22	0.039	0.10
IVB	0.21	0.050	0.057	0.025	0.014	0.050

Determination of the longitudinal response function becomes increasingly difficult with increasing $\vec{q}$ due to the error magnification in performing the separation from the individual cross sections. In Table 8 the uncertainties in R_L and R_T are

given assuming statistical uncertainties of 1% in the cross sections as well as for the systematic uncertainties computed above. The systematic errors tend to be small at zero recoil since we are at a turning point in the momentum distribution. These errors also assume the values of R_L/R_T given by our model calculation at the central kinematics. One percent measurements of the cross sections (total uncertainty) would provide a 22% measurement of R_L at the highest $\vec{q}$ studied. Although the kinematical domain accessible to CEBAF is somewhat larger, $\sim$ 3 GeV/c appears to be the practical limit for these separation measurements.

Table 8

Errors in Response Functions

$\vec{q}$ GeV/c	R_L/R_T	$\delta R_L/R_L$ (%) statistical	$\delta R_T/R_T$ (%) statistical	$\delta R_L/R_L$ (%) systematic	$\delta R_T/R_T$ (%) systematic
0.5	1.000	2.6	2.5	0.63	0.37
1.0	0.309	4.5	1.3	0.84	0.08
1.9	0.139	12	1.2	1.2	0.06
2.6	0.116	22	1.3	1.8	0.07

6 Proton Angular Distribution Measurement

Next, a measurement of the angular distribution of protons for recoil momenta up to 500 MeV/c is described for a single momentum transfer of $\vec{q}$ = 1 GeV/c. The invariant mass is held constant and the kinematics are quasifree (x = 1). By making measurements on either side of the $\vec{q}$ direction the R_{LT} interference response function can be isolated. Denoting the measured cross section by σ, then

$$\sigma_{LT} = \left[\sigma(\phi_z = 0) - \sigma(\phi_z = \pi)\right]/2.$$

In addition, the R_T response function can be separated by making an additional measurement at a backward electron angle. The cross sections are calculated for eight kinematics centered at recoil momenta of 0, 50, 100, 150, 200, 300, 400 and 500 MeV/c. The actual measurements will be made by moving the spectrometer in a set of overlapping steps allowing a uniform measurement of the response functions as a function of recoil momentum or angle. The p_r = 0 point is at the

Table 9A

Forward Angle

Kinematics for Proton Angular Distribution Measurement

$E_{pn}^{cm} = 206$ MeV $\quad \vec{q}_{cm} = 901$ MeV/c

$\vec{q}$ GeV/c	e MeV	ω MeV	θ deg	ϵ
1.0	4000.0	435.2	13.69	0.966
Kin	p_r MeV/c	T_p MeV	θ_p deg	θ_{pn}^{cm} deg
0	0	433.0	−57.55	0
50A	50	431.7	−54.68	6.36
50B			−60.42	
100A	100	427.7	−51.81	12.72
100B			−63.29	
150A	150	421.1	−48.93	19.08
150B			−66.17	
200A	200	412.0	−46.02	25.49
200B			−69.08	
300A	300	386.3	−40.13	38.36
300B			−74.97	
400A	400	351.4	−33.05	51.47
400B			−81.05	
500A	500	308.2	−27.69	64.94
500B			−87.41	

same kinematics as for the L/T separation (kinematics IIF/IIB). The proton final momentum and angle are correlated for fixed electron kinematics and were varied to achieve the desired value of p_r. This technique minimizes the variations in the final-state interaction. Tables 9A and 9B summarize the kinematics.

Integrated cross sections and counting rates are given in Tables 10 and 11 respectively. Counting rates assume a luminosity of 1.4×10^{38} cm^{-2}sec^{-1} as before. The signal-to-noise ratio is 0.63 for the worst case after inclusion of vertex and missing mass resolution cuts. The highest recoil momentum measurements would be severely signal-to-noise limited if it were not for the excellent traceback properties

Table 9B

Backward Angle

Kinematics for Proton Angular Distribution Measurement

$E_{pn}^{cm} = 206$ MeV $\quad \vec{q}_{cm} = 901$ MeV/c

$\vec{q}$ GeV/c	e MeV	ω MeV	θ deg	ϵ
1.0	800.0	435.2	112.88	0.151
Kin	p_f MeV/c	T_p MeV	θ_p deg	θ_{pn}^{cm} deg
0C	1000.0	433.0	−19.64	0
50C	998.2	431.7	−22.51	6.36
100C	992.7	427.7	−25.38	12.72
150C	983.6	421.1	−28.62	19.08
200C	970.9	412.0	−31.17	25.49
300C	934.9	386.3	−37.06	38.36
400C	884.8	351.4	−43.14	51.47
500C	820.6	308.2	−49.50	64.94

of the Hall A spectrometer pair. The missing mass and vertex resolution improves the signal-to-noise ratio by a factor of 360.

In order to restrict the electron kinematics to the quasielastic peak and for comparison to the previous set of experiments, coincidence rates were calculated with a cut on ω: $417 \leq \omega \leq 453$ MeV, and on the angular range of $\vec{q}$ as in Kinematics II. The resulting coincidence rates and counting times are given in Table 12. Counting times are based on 1% statistics overall except for Kinematics 500C where 2% statistics are assumed. Also shown are the ranges of p_r covered.

In general, the extraction of the momentum distribution can only be done in the context of some reaction model. Relative to a single-particle knockout model the effective momentum distribution can be sensitive to the choice of kinematics. For example, at high recoil momentum (~ 500 MeV/c) virtual Δ channels can affect the results by as much as a factor of two for some kinematics.[3] Therefore, follow-up measurements to study the systematics of the reaction process would be greatly desired.

Table 10

Cross Sections for Angular Distribution Measurement

(e,e′) Kin. A,B: 186 Kin. C: 0.818 nb/sr

(e,π^-) Kin. A,B: 15.5 Kin. C: 0.249 nb/sr

Kin	(e,p) nb/sr	(e,π^+) nb/sr
0A,B	39.6	26.8
0C	24.2	0.
50A	101	27.7
50B	1.29	26.0
50C	5.49	0.
100A	114	28.5
100B	175	25.3
100C	2.22	0.
150A	125	28.9
150B	304	24.1
150C	2.08	0.
200A	139	29.9
200B	409	23.3
200C	2.05	0.
300A	163	31.0
300B	517	13.7
300C	2.23	0.
400A	193	31.8
400B	470	3.68
400C	2.86	0.
500A	226	32.7
500B	322	0.
500C	4.19	0.

The results of a sensitivity analysis are given in Table 13. Both the electron incident and final energy must be determined to $\sim 1 \times 10^{-4}$ to restrict the uncertainty with respect to each of these variables separately to 1%. The angles of the beam, scattered electron and proton must all be determined to $\sim 0.1 - 0.2$ mr for a 1% uncertainty as well. Clearly, this assumes the presence of beam position monitors

Table 11

Counting Rates for Angular Distribution Measurement

(e,e') Kin. A,B: 205000 Kin. C: 900 sec^{-1}

(e,e') Kin. A,B with ω cut: 109000

(e,π^-) Kin. A,B: 17000 Kin. C: 275 sec^{-1}

Kin	(e,p) sec^{-1}	(e,π^+) sec^{-1}	trues sec^{-1}	accid. sec^{-1}	S/N
0A,B	43600	29500	3750	0.0265	142000
0C	26600	0	384	0.000133	2880000
50A	111000	30400	2260	0.0673	33600
50B	1420	9370	2140	0.000863	2480000
50C	6050	0	180	0.0000303	5940000
100A	126000	31400	603	0.0750	8040
100B	193000	27800	604	0.117	5160
100C	2440	0	33	0.0000122	2700000
150A	138000	31800	151	0.0835	1810
150B	335000	26500	170	0.203	837
150C	2290	0	6.59	0.0000111	594000
200A	153000	32900	42	0.0928	453
200B	450000	25600	54.9	0.273	201
200C	2260	0	1.65	0.0000111	149000
300A	180000	34100	4.33	0.109	39.7
300B	569000	15100	7.88	0.345	22.8
300C	2460	0	0.171	0.0000122	14000
400A	213000	35000	0.437	0.129	3.39
400B	518000	4050	1.51	0.314	4.81
400C	3150	0	0.0268	0.0000157	1710
500A	249000	36000	0.0951	0.151	0.630
500B	355000	0	0.348	0.215	1.62
500C	4620	0	.00525	0.0000231	227

with excellent spatial resolution. With the assumed measurement uncertainties, systematic errors are seen to be ~2% or less. The errors are largest where the momentum distribution is most rapidly varying.

Table 12

Coincidence Rates and Counting Times with Cuts

$417 \leq \omega \leq 453$ MeV

Kin	$\lvert\vec{p}_r\rvert$ Range MeV/c	trues sec^{-1}	Time ($L_{max} = 75\mu$A-g/cm^2) hours
0A,B	0–100	3750	< 0.1
0C		384	< 0.1
50A	0–100	2260	< 0.1
50B		2140	< 0.1
50C		180	< 0.1
100A	50–150	603	< 0.1
100B		604	< 0.1
100C		33	< 0.1
150A	100–200	151	< 0.1
150B		170	< 0.1
150C		6.59	0.4
200A	150–250	42	0.1
200B		54.9	< 0.1
200C		1.65	1.7
300A	250–350	4.33	0.7
300B		7.88	0.4
300C		0.171	16.3
400A	350–450	0.437	8.3
400B		1.51	2.3
400C		0.0268	104
500A	450–550	0.0951	75.5
500B		0.348	13
500C		0.00525	**132
TOTAL			355.8
TOTAL incl. rad. corr.			437

** reduced statistics to ± 2%

7 Experimental Equipment

This experiment is proposed with the two high resolution spectrometers in mind,

Table 13

Systematic Uncertainties in Cross Section

Kin	e %/MeV	θ_b %/mr	e' %/MeV	θ %/mr	θ_p %/mr	Total Error %
0A,B	0.53	0.64	0.17	0.19	0.13	0.23
0C	0.54	0.060	0.064	0.0070	0.059	0.044
50A	3.6	13	3.4	0.80	4.4	2.3
50B	4.2	7.3	3.7	0.22	4.0	2.3
50C	2.2	3.3	1.7	1.2	4.1	0.57
100A	3.0	12	3.4	2.4	4.2	2.1
100B	3.4	4.4	3.4	0.41	3.8	1.9
100C	1.9	2.6	1.8	1.2	3.9	0.51
150A	2.4	11	2.8	4.0	3.4	1.8
150B	2.8	2.4	2.8	0.78	3.0	1.6
150C	1.7	1.9	1.3	1.0	3.0	0.40
200A	2.0	10	2.5	5.4	2.8	1.7
200B	2.3	0.65	2.3	1.4	2.6	1.3
200C	1.6	1.6	1.0	0.95	2.6	0.35
300A	1.4	9.2	1.8	5.9	2.2	1.4
300B	1.9	0.69	1.8	2.2	1.9	1.1
300C	1.5	1.1	0.51	0.84	2.0	0.27
400A	0.93	8.4	1.3	6.2	1.7	1.2
400B	1.6	1.8	1.5	2.9	1.5	0.91
400C	1.4	0.77	0.13	0.78	1.6	0.22
500A	0.69	7.9	1.1	6.2	1.4	1.1
500B	1.4	2.6	1.2	3.5	1.3	0.83
500C	1.3	0.55	0.16	0.73	1.3	0.19

as proposed by the Hall A collaboration. The high resolution capabilities of the spectrometers are essential in carrying out this experiment. In particular, an analysis of systematic errors indicates that very good incident energy, final electron momentum and in-plane angular determinations are required for high precision separation measurements. In addition, in order to maintain a favorable signal-to-noise ratio at high recoil momenta, good missing mass and vertex resolution are required. The dynamic range of this experiment requires spectrometers with a

momentum range of ~ 0.3 GeV/c to 4 GeV/c with a premium on reaching small angles.

A schematic diagram of the focal plane detectors for the hadron arm is given in Figure 8.[26] We plan to use pairs of vertical drift chambers to determine the final particle trajectories. Because of the rapid variation of the coincidence cross section across the acceptance, the focal plane must be uniform and well understood. Additional instrumentation is required for accurate timing and particle identification. In particular, pion rejection in the electron arm will require the use of both Čerenkov and shower counters.

To minimize running times, high luminosity and the ability to view extended targets is required. The Hall A collaboration is developing high power liquid targets capable of sustaining full beam current on an extended target cell of 10–15 cm. For this proposal we have limited the beam current to 50μA because of precision requirements. Even so, at the lower momentum transfers beam currents will have to be reduced slightly to avoid data acquisition and data processing bottlenecks. However, the effect on the total time estimate is negligible. The instrumentation should be capable of handling instantaneous singles rates on the order of 1 MHz and coincidence rates on the order of 10 KHz.

Details of the spectrometers and instrumentation can be found in the Hall A Conceptual Design Report.

8 Beam Time Summary

The beam time needed to complete these measurements is shown in Table 14. The 19 hours estimated for the L/T measurement is somewhat deceiving since for short runs, overhead dominates data acquisition times. Although an operating scenario has not yet been worked out for CEBAF we have estimated a one hour overhead associated with each angle/field change. In addition, based on previous experience about 48 hours will be required for calibration and normalization measurements. With targets capable of handling luminosities of 75 μA-g/cm^2 the total beam time is 554 hours. We expect that the program on D(e,e'p) will form the basis of a number of Ph.D. theses with 2 to 4 theses resulting from this initial study.

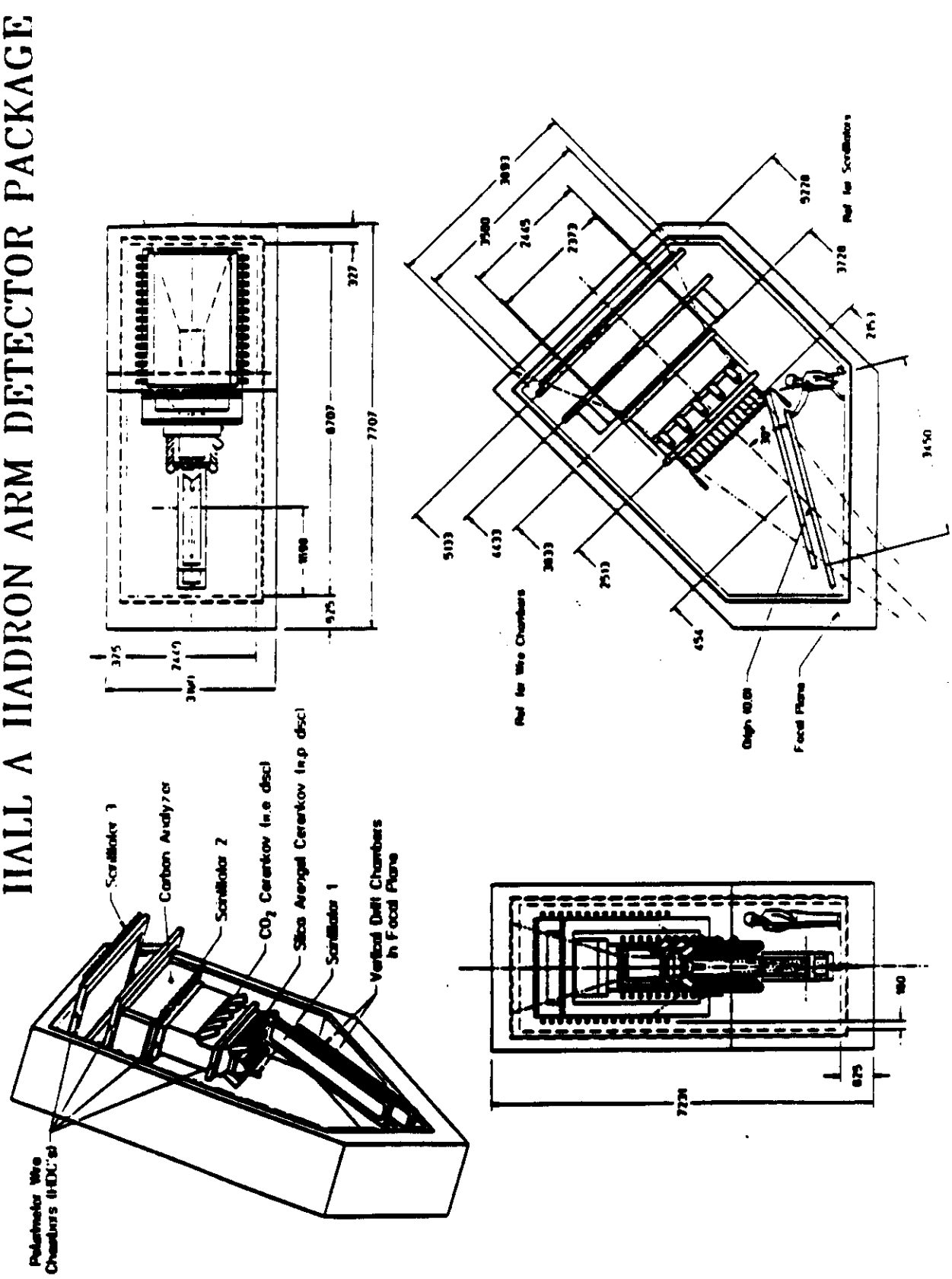

Figure 8 Schematic diagram of the focal plane instrumentation package for the hadron arm.

Table 14

Beam Time Summary

Measurement	time (hours)
R_L/R_T	19
Angular Distribution	437
Norm./Calib.	48
Field/Angle changes	50
TOTAL	554

References

[1] T. Tamae *et al.*, Phys. Rev. Lett. **59**, 2919 (1987).

[2] M. Bernheim *et al.*, Nucl. Phys. **A365**, 349 (1981).

[3] S. Turck-Chieze *et al.*, Phys. Lett. **142B**, 145 (1984).

[4] M. van der Schaar, private communication.

[5] Bates proposal # 87-07, *A Measurement of the f_{-11} Structure Function in the D(e,e'p) Reaction*; Bates proposal # 88-19, *Determination of the Longitudinal and Transverse Structure Functions in the D(e,e'p) Reaction.*

[6] V. Punjabi *et al.*, Phys. Rev. **C38**, 2728 (1988); V. Punjabi, Ph.D. Thesis, The College of William and Mary, (1986).

[7] M. Gourdin, Nuovo Cim. **21**, 1094 (1961).

[8] A. Picklesimer and J.W. Van Orden, Phys. Rev. **C35**, 266 (1987).

[9] W. Fabian and H. Arenhövel, Nucl. Phys. **A314**, 253, (1979).

[10] H. Arenhövel, private communication.

[11] A. Yu. Korchin, Yr. P. Mel'nik and A.V. Shebeko, Yad. Fiz. **48**, 387 (1988); M.P. Rekalo, G.I. Gakh and A.P. Rekalo, J. Phys. G. **15**, 1223 (1989); J.M. Laget, private communication.

[12] J.W. Van Orden and F. Gross, private communication.

[13] P.E. Ulmer *et al.*, Phys. Rev. Lett. **59**, 2259 (1987).

[14] G. van der Steenhoven *et al.*, Phys. Rev. Lett. **57**, 182 (1986).

[15] D. Reffay-Pikeroen *et al.*, Phys. Rev. Lett. **60**, 776 (1988).

[16] C. Ciofi degli Atti, O. Benhar and G. Salmé, Proc. of the Fourth Miniconference, NIKHEF-K (1985).

[17] J.W. Lightbody and J.S. O'Connell, Computers in Physics, May/June 1988, p. 57.

[18] L.E. Wright and L. Tiator, Phys. Rev. C **26**, 2349 (1982).

[19] A.E. Thorlacius and H.W. Fearing, Phys. Rev. C **33**, 1830 (1986).

[20] P.E. Ulmer, Computer Program MCEEP (1989).

[21] S. Frullani and J. Mougey, *Advances in Nuclear Physics*, vol. 14, ed. by J.W. Negele and E. Vogt, Plenum Press (1985).

[22] T. de Forest, Jr., Nucl. Phys. **A392**, 232 (1983).

[23] F. Krautschneider, Ph.D. Thesis, Bonn University, BONN-IR-76-37 (1976); L. Hulthen and M. Sagawara, Handb. d. Phys. Bd. 39, S.1.

[24] M. Lacombe *et al.*, Phys. Lett. **101B**, 139 (1981).

[25] P.E. Ulmer, Computer Program SIGEEP (1987).

[26] CEBAF Hall A Conceptual Design Report (1989).